BIOCHEMISTRY
including biophysical chemistry & molecular biology

Article

pubs.acs.org/biochemistry

WW Domain Folding Complexity Revealed by Infrared Spectroscopy

Caitlin M. Davis and R. Brian Dyer*

Department of Chemistry, Emory University, Atlanta, Georgia 30322, United States

Supporting Information

ABSTRACT: Although the intrinsic tryptophan fluorescence of proteins offers a convenient probe of protein folding, interpretation of the fluorescence spectrum is often difficult because it is sensitive to both global and local changes. Infrared (IR) spectroscopy offers a complementary measure of structural changes involved in protein folding, because it probes changes in the secondary structure of the protein backbone. Here we demonstrate the advantages of using multiple probes, infrared and fluorescence spectroscopy, to study the folding of the FBP28 WW domain. Laser-induced temperature jumps coupled with fluorescence or infrared spectroscopy have been used to probe changes in the peptide backbone on the submillisecond time scale. The relaxation dynamics of the β-sheets and β-turn were measured independently by probing the corresponding IR bands assigned in the amide I region. Using these wavelength-dependent measurements, we observe three kinetics phases, with the fastest process corresponding to the relaxation kinetics of the turns. In contrast, fluorescence measurements of the wild-type WW domain and tryptophan mutants exhibit single-exponential kinetics with a lifetime that corresponds to the slowest phase observed by infrared spectroscopy. Mutant sequences provide evidence of an intermediate dry molten globule state. The slowest step in the folding of this WW domain is the tight packing of the side chains in the transition from the dry molten globule intermediate to the native structure. This study demonstrates that using multiple complementary probes enhances the interpretation of protein folding dynamics.

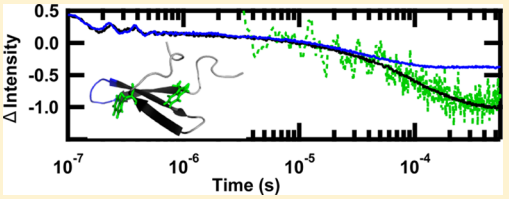

One of the most convenient probes of protein structure is the intrinsic fluorophore tryptophan. However, interpretation of tryptophan fluorescence is difficult because it can be sensitive to either local or global changes or both. Furthermore, introduction of new tryptophan probes into a protein structure may perturb the structure and the folding dynamics and mechanism. A complementary approach is infrared spectroscopy of the amide I mode of the peptide backbone. The advantage of using vibrational spectroscopy is that the spectral features are local; different regions of the amide I′ band report on different parts of a folded peptide or protein. Using infrared spectroscopy to independently probe the portion of the peptide assigned to different secondary structure elements, it should be possible to determine the folding dynamics with a resolution greater than that of fluorescence spectroscopy.[1] β-Proteins are naturally composed of two secondary structure elements, the turn and β-sheet. The turns are thought to act as nucleation sites for the folding of the larger β-protein.[2] Via comparison of the dynamics when the turn and β-sheet are probed, it should be possible to identify whether the turn and β-sheet form concurrently or with a specific ordering.

Here we have compared time-resolved measurements probed by fluorescence and infrared in one of the fastest folding β-protein families, the WW domain. The WW domain family consists of an antiparallel and highly twisted three-stranded β-sheet structure with a small hydrophobic core and two highly conserved tryptophan residues.[3−6] Because of the fast, submillisecond folding and native tryptophan fluorescence, WW domains have been the focus of extensive computational and experimental studies.[7−17] Studies of the Formin Binding Protein 28 (FBP28) WW domain (Figure 1) have proposed different folding models involving either three states[10,11,14,18] or two states.[9,15,16,19] In many of the experimental studies, laser-induced temperature jumps probed by fluorescence were used

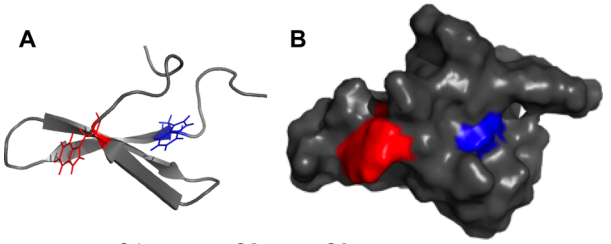

Figure 1. (A) Cartoon and (B) space filling model of the FBP28 WW domain (Protein Data Bank entry 1E0L) showing the Trp8 (blue) and Trp30 (red) residues. Below is shown the mutated protein sequence, FBP28, compared to the wild-type sequence, WTFBP28. The three β-sheets are labeled above and underlined in the WTFBP28 sequence. Mutations (bold), Trp8 (blue), and Trp30 (red) are highlighted in the FBP28 sequence. This figure was prepared with PyMOL (http://www.pymol.org).

Received: May 9, 2014
Revised: August 8, 2014
Published: August 14, 2014

   dx.doi.org/10.1021/bi500556h | *Biochemistry* 2014, 53, 5476−5484

to determine the folding kinetics.[9,14−16] We employed two approaches to increase the structural resolution of the temperature jump measurements. In the first approach, infrared spectroscopy was used to independently probe the dynamics of the turn and β-sheet. In the second approach, tryptophan mutations were introduced to create a more localized fluorescent probe.

Mutation of the two conserved tryptophans in the FBP28 WW domain has been performed with varying degrees of success.[14,16] The tryptophan in the second loop, Trp30, has been shown to be more amenable to mutation than the tryptophan in the first loop, Trp8, likely because Trp8 is buried in the hydrophobic core of the WW domain. Mutation of Trp8 to glycine or alanine completely destabilized the WW domain, whereas mutation to another aromatic residue, phenylalanine, still allowed folding into a WW domain.[16] Similarly, mutation of Trp30, located in the second loop, to phenylalanine had a slight stabilizing affect compared to the effect of mutation to alanine, which was slightly destabilizing.[14] On the basis of these observations, we concluded that mutation of the tryptophans to another aromatic group preserves the aromatic packing necessary for the protein to fold. Therefore, we investigated fluorescent mutants in which the tryptophans are individually replaced with the aromatic residue tyrosine, W8Y and W30Y.

We compared the stability and folding kinetics of the wild-type and mutated WW domains. The stability of the WW domains was determined by equilibrium circular dichorism and Fourier transform infrared (FTIR) measurements. The dynamics of WW domain formation was measured using temperature jump, time-resolved infrared and fluorescence spectroscopy. Pulsed laser excitation was used to rapidly initiate a shift in the folding equilibrium. The relaxation of the WW domains was measured by both an infrared probe and a fluorescence probe. The dynamics of the β-sheets and turns were independently measured by probing the components of the IR amide I band assigned to each structure. We found that mutation of Trp8 resulted in a destabilization of the peptide and a less rigid hydrophobic core. Because FBP28 W8Y does not fold with a tightly packed core, the slowest step in folding is eliminated in this case, and therefore, its folding rate is 1 order of magnitude faster than those of the other systems studied here. As expected, mutation of Trp30 had little effect on the protein's stability. Both mutants and the wild-type system exhibited multiexponential behavior upon being probed by infrared spectroscopy, but only one phase upon being probed by fluorescence.

These experiments demonstrate the importance of using multiple probes to determine protein dynamics. Wavelength-dependent infrared measurements reveal a fast 100 ns phase, an intermediate microsecond phase, and a slow phase of hundreds of microseconds. These measurements provide direct evidence of a mechanism of WW domain formation initiated in the turns. The single phase observed by fluorescence coincides with the slowest phase observed by infrared spectroscopy. Tryptophan mutants enhance our understanding of the dynamics of the hydrophobic core. They suggest that there is an intermediate dry molten globule state prior to the rearrangement of the tryptophan residues in the hydrophobic core of the WW domain. These results demonstrate the value of multiple spectroscopic probes in providing a more complete view of the mechanism of protein folding.

EXPERIMENTAL SECTION

Protein Synthesis and Purification. FBP28 (Figure 1) and tryptophan mutants were synthesized via standard 9-fluorenylmethoxycarbonyl (Fmoc)-based solid-phase chemistry on a Liberty1 microwave peptide synthesizer (CEM, Matthews, NC). Fmoc-PAL-PS resin (Applied Biosystems, Foster City, CA) was used to form a peptide amide. The peptide was purified by reverse-phase chromatography (C18 column) using a water/acetonitrile gradient with 0.1% trifluoroacetate (TFA) as the counterion. TFA interferes in the amide I IR measurements at 1672 cm^{-1}, so we remove it by anion exchange. The peptide was lyophilized and dissolved in a 2 mM HCl solution to allow exchange of the TFA counterion for chloride.[20] The identity of the peptide was confirmed by matrix-assisted laser desorption ionization time-of-flight mass spectrometry. The peptide was lyophilized and dissolved in D_2O to allow deuterium−hydrogen exchange of the amide protons. The peptide was lyophilized a second time and resuspended in D_2O buffer with 20 mM potassium phosphate buffer at pD* 7.0 (pD* refers to the uncorrected pH meter reading). Sample concentrations of 0.5−1.0 mM were prepared for both IR and fluorescence experiments.

Circular Dichroism (CD) Spectroscopy. CD spectra and CD melting curves were recorded on a Jasco J-810 spectropolarimeter equipped with a PFD-425S Jasco temperature controller module (Jasco, Inc., Easton, MD). Peptides were dissolved at a concentration of 50 μM in 20 mM potassium phosphate buffer (pH 7.0). All measurements were taken using a 1 mm path length cell. Wavelength scans were recorded over the range from 260 to 190 nm with an average of three repeats. A bandwidth of 2 nm and a scan rate of 50 nm/min were used for spectral acquisition. Thermal unfolding experiments were performed by monitoring the signal at 226 nm from 5 to 90 °C using a 0.1 °C interval and a scan rate of 30 °C/h. During the thermal unfolding experiment, a full wavelength scan was obtained every 5 °C after a 60 s delay. The buffer and protein concentrations were the same as those used in the wavelength scan experiment.

FTIR Spectroscopy. The equilibrium melting behavior was monitored on a Varian Excalibur 3100 FTIR spectrometer (Varian Inc., Palo Alto, CA) using a temperature-controlled IR cell. The IR cell consists of two CaF_2 windows stacked and separated by a 100 μm Teflon spacer split into two compartments, a sample and a reference. The same cells are used for equilibrium FTIR and *T*-jump experiments. No aggregation was observed in the infrared at the reported concentrations. All spectra shown at a specific temperature were constructed by subtracting the spectrum of the reference buffer solution without protein from the spectrum of the sample solution with protein. The temperature-dependent difference spectra were then generated by subtracting the spectrum at the lowest temperature from the spectra at higher temperatures. The second-derivative spectra were computed in IGOR PRO after smoothing the data with a sixth-order binomial algorithm to remove any residual water vapor (WaveMetrics, Lake Oswego, OR).

Time-Resolved Temperature Jump (*T*-jump) Relaxation Measurements. The IR *T*-jump apparatus has been described previously.[21] Pulsed laser excitation is used to rapidly perturb the folding equilibrium on a time scale faster than the molecular dynamics of interest. Time-resolved infrared is then used to probe the reaction. A Q-switched DCR-4 Nd:YAG laser

dx.doi.org/10.1021/bi500556h | *Biochemistry* 2014, 53, 5476−5484

(Spectra Physics, Mountainview, CA) fundamental at 1064 nm is Raman-shifted (one Stokes shift in 200 psi of H_2 gas) to produce a 10 ns pulse at 2 μm. The magnitude of the T-jump is calculated using the change in reference absorbance with temperature. The T-jump reference is taken from D_2O buffer with 20 mM potassium phosphate buffer (pD* 7.0) at the same temperature and frequency that were used for the sample. Absorbance changes at the reference frequency are due only to changes in D_2O absorbance, which is used as an internal thermometer.[21]

The change in signal induced by the T-jump is probed in real time by a continuous laser with a frequency in the amide I′ band of the IR or at 285 nm to excite Trp fluorescence. The mid-IR probe beam is generated by a continuous wave quantum cascade laser (Daylight Solutions Inc., San Diego, CA) with a tunable output range of 1570−1730 cm^{-1}. The transient transmission of the probe beam through the sample is measured using a fast, 100 MHz, photovoltaic MCT IR detector/preamplifier (Kolmar Technologies, Newburyport, MA). Transient signals are digitized and signal averaged (1000 shots) using a Tektronics (Beaverton, OR) model 7612D digitizer.

The fluorescence excited at 285 nm and collected from 320 to 370 nm is sensitive to changes in the tryptophan residues. A Verdi V12 DPSS high-power continuous wave laser (Coherent, Santa Clara, CA) is used to pump a Mira 900 Ti:Saph laser (Coherent) that produces a quasi-continuous beam at 855 nm. The beam is then passed through a second and third harmonic generator (Coherent) to produce the fluorescence probe beam at 285 nm. The back-emitted fluorescence light induced by the 285 nm pump laser is measured using a Hamamatsu R7518 photomultiplier tube (Hamamatsu Photonics K. K., Hamamatsu City, Japan), digitized, and signal averaged (5000 shots) using a Tektronics model 7612D digitizer. A 400 μM tryptophan (Trp) solution in D_2O is used as a reference to measure the magnitude of the temperature jump and determine the temperature dependence of the tryptophan signal. Instrument control and data collection are controlled using a LabVIEW computer program (National Instruments, Austin, TX).

Analysis of Kinetic Data. The peptide relaxation kinetics must be deconvolved from the observed kinetics. Accurate deconvolution is possible as the instrument response is determined from the reference measurement under the exact conditions of the sample measurements. To minimize detector artifacts, the reference is scaled prior to subtraction from the sample. The decay function is a triple-exponential decay with the formula

$$A = A_0 + \ldots + A_n \exp\left[\frac{-(x - x_0)}{\tau_n}\right] \quad (1)$$

where A_0 is an offset, n is the number of exponentials to fit, A_n is a preexponential factor, τ_n is the relaxation lifetime of the sample, and x_0 is the time offset. To best fit the data, the minimal number of exponentials with unique relaxation lifetimes was selected. The data are fit over the interval from 90 ns to 1 order of magnitude outside the slowest exponential. In the cases where a fast phase is not reported, the fit starts at 400 ns. Fluorescence measurements are fit starting at 5 μs. Data analysis was performed in IGOR PRO.

RESULTS AND DISCUSSION

Far-UV CD Spectroscopy. The CD spectra of wild-type FBP28 and, to a lesser extent, the FBP28 W30Y and FBP28 W8Y mutants exhibit a positive peak at 226 nm and a negative peak at 197 nm (Figure 2A). The typical β-sheet spectrum has a negative peak at ∼218 nm and a positive peak at ∼195 nm.[22] Spectra of folded WW domains instead have a negative peak at ∼202 nm and a positive peak at ∼230 nm that provides a distinct CD signature.[23,24]

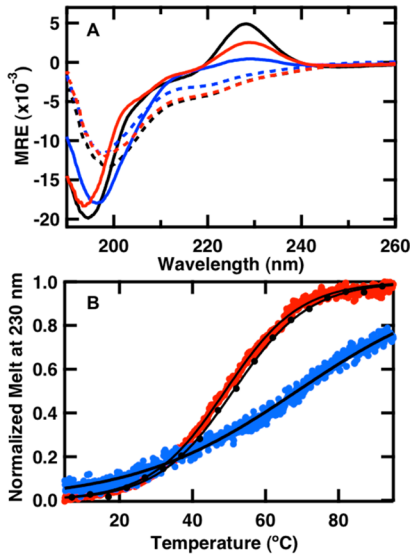

Figure 2. (A) Far-UV CD spectra of 50 μM solutions of FBP28 (black), FBP28 W8Y (blue), and FBP28 W30Y (red) WW domains in 20 mM potassium phosphate buffer (pD 7.0) acquired at 5 (solid lines) and 95 °C (dashed lines) during the course of a thermal denaturation in a 0.1 cm path length cell. (B) Thermal denaturation of the WW domains monitored by CD at 226 nm. The solid line is a fit to an apparent two-state model (eq 2) that was then normalized.

Small variations in the position and intensities of these peaks have been observed among members of the WW domain family.[24] The peak at ∼202 nm resembles the random coil peak usually found at 200 nm. Disorder in the N- and C-termini of the folded structure of WW domains is thought to contribute to the negative peak in the CD spectrum.[23,25−27] The peak at ∼230 nm arises from the presence of ordered aromatic side chains.[9,22,23] Therefore, the CD spectra of FBP28 and the tryptophan mutants are consistent with a WW domain topology.

Mutation of Trp8 or Trp30 results in a reduction in the intensity of the 226 nm peak. FBP28 W30Y exhibits a cooperative thermal denaturation detected by CD (Figure 2B) that closely resembles that of wild-type FBP28. This is further evidence that the W30Y mutant adopts a WW domain structure. Thus, the diminished 230 nm CD signal of the FBP28 W30Y mutant compared to that of wild-type FBP28 can be attributed to the absence of Trp30. A similar mutation to loop 2 of the human Pin1 WW domain was confirmed to be a WW domain based on the same observations, supporting this assignment.[28] FBP28 W8Y exhibits a weak feature at 230 nm with a broad, noncooperative dependence on temperature (Figure 2). WW domains include a conserved Trp8-Tyr20-Pro33 hydrophobic core.[14] Apparently, mutation of Trp8 disrupts this core, affecting the packing of the entire domain. In

dx.doi.org/10.1021/bi500556h | Biochemistry 2014, 53, 5476−5484

this mutant, the observed CD band at 226 nm must be due to Trp30. The expected contribution of Trp30 to the 226 nm CD signal for the correctly folded WW domain is obtained from the difference between the wild-type (WT) and W30Y mutant CD spectra shown in Figure 2A. The weak feature at 226 nm observed for the W8Y mutant is not consistent with the expected contribution of Trp30 in the folded state. This suggests that the environment of the tryptophan in the outer loop is not rigid, supporting our observation that the fold is disrupted by the W8Y mutation.

Thermal denaturation was monitored by recording the absorbance change at 230 nm with temperature (Figure 2B). The WW domains exhibit the typical heat-induced unfolding behavior with a loss of intensity at 226 nm and a shift of the minimum from 197 to 200 nm, corresponding to a change in the secondary structure from the WW domain to the random coil (Figure 2A).[23] The melting curves (Figure 2B) were fit to an apparent two-state equilibrium model:

$$A_O = \frac{A_F}{1 + \exp\left[-\frac{\Delta H}{R}\left(\frac{1}{T} - \frac{1}{T_m}\right)\right]} + \frac{A_U}{1 + \exp\left[\frac{\Delta H}{R}\left(\frac{1}{T} - \frac{1}{T_m}\right)\right]} \quad (2)$$

where A_O is the observed absorbance, A_F and A_U are the absorbance contributions from the folded and unfolded populations, ΔH is the enthalpy change at the midpoint, R is the gas constant, and T_m is the transition midpoint.[29] This analysis assumes a ΔC_p of 0 as it is unlikely that a small peptide like a WW domain would have a large difference in heat capacity between the folded and unfolded states. The data are then normalized for comparison. The observed melting temperature of wild-type FBP28 is 51.1 ± 0.3 °C. This agrees with the previously reported melting temperature of FBP28, 50.9 °C, obtained by an infrared melt of the β-sheet band at 1636 cm^{-1}.[30] The melting temperature of the FBP28 W30Y mutant is 49.0 ± 0.1 °C. The W30Y mutation results in a decrease in the melting temperature of ~2 °C. The breadths of the transition of FBP28 and FBP28 W30Y are the same, showing that while the mutation results in a slight destabilization, the cooperativity of the folding transition is unchanged (Figure 2B). The transition of FBP28 W8Y was too broad to obtain a reliable fit. This is evidence that mutation of Trp8 results in destabilization of the fold such that the transition becomes less cooperative.

FTIR Spectroscopy. The temperature-induced unfolding of FBP28 and the tryptophan mutants was studied over the range from 5 to 85 °C in 5 °C intervals using FTIR spectroscopy to monitor the amide I′ region. An example of the temperature-dependent absorption spectra of the amide I′ spectral region (amide I region of peptides in D_2O) of FBP28 is shown in Figure 3A (see tryptophan mutants in Figure S1 of the Supporting Information).

The amide I′ absorbance arises from C═O stretching vibrations of the polypeptide backbone carbonyls and is an established indicator of secondary structure.[31−33] This relatively broad band contains contributions from the entire polypeptide backbone, which in the case of the WW domain includes β-sheet, β-turn, and random coil structure. The changes with temperature are highlighted by the difference spectra for each peptide (Figure 3B). The difference spectra are generated by

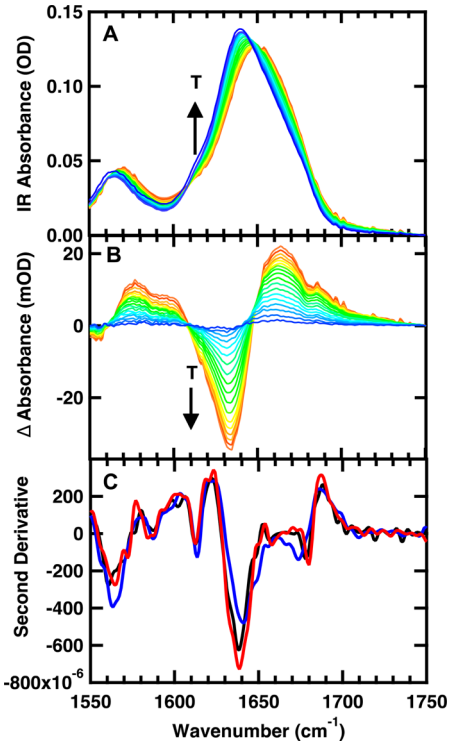

Figure 3. Temperature-dependent FTIR spectra of 1 mM FBP28 in 20 mM potassium phosphate buffer (pH 7). (A) Absorbance spectra in the amide I′ region. The temperature of the individual traces varies from 5 to 85 °C in 5 °C intervals. (B) Difference spectra obtained by subtracting the spectrum at 5 °C from the spectra at higher temperatures. (C) Second derivative of the FTIR absorbance spectrum of FBP28 (black), FBP28 W8Y (blue), and FBP28 W30Y (red) WW domains at 5 °C.

subtracting the lowest-temperature spectrum from each absorbance spectrum at higher temperatures. Negative peaks correspond to specific structures or interactions present in the folded state, and positive peaks correspond to new interactions with solvent in the unfolded state. The individual peaks are more easily distinguished in the second derivative of the FTIR spectra at the lowest temperature (Figure 3C).

This analysis reveals three main components of the amide I′ band at 5 °C, centered at 1613, 1638, and 1678 cm^{-1}. The intensity of these features decreases with an increase in temperature, meaning that they are all associated with the folded state. These peaks have previously been observed in other WW domains.[18,34] A peak at ~1611 cm^{-1} in β-hairpins has been assigned to an amide C═O group in the turn usually involved in multiple hydrogen bonds with side chain or backbone donors.[35,36] There is one such group in the first turn and none in the second turn of the wild-type FBP28 WW domain.[4,37] We assign the peak at 1613 cm^{-1} to the backbone amide I′ mode of threonine 13, which is strongly hydrogen-bonded to the backbone NH groups of glycine 16 and lysine 17 in the first turn of the WW domains. This peak is of equal intensity in all three peptides (Figure 3C) as all three peptides contain the same first turn. IR bands at 1634 and 1681 cm^{-1} are well-established components of antiparallel β-sheets.[38] The amide I band is split into a peak at 1681 and 1634 cm^{-1} due to out-of-phase and in-phase C═O stretching of neighboring amides. The efficiency of interstrand coupling depends on the orientation of the dipole moments of the individual carbonyl oscillators. Misaligned carbonyl oscillators do not couple as

dx.doi.org/10.1021/bi500556h | Biochemistry 2014, 53, 5476−5484

efficiently, leading to a decrease in the magnitude of splitting. The splitting is sensitive to the number of strands in a β-sheet; as the number decreases, the amide I splitting and intensity also decrease.[38] The FBP28 and FBP28 W30Y amide I′ bands at 1638 and 1678 cm^{-1} are consistent with these characteristic β-sheet markers. The β-sheet peaks of the FBP28 W8Y mutant have decreased intensity and splitting, such that they are shifted to 1641 and 1673 cm^{-1} (Figure 3C). One interpretation of the FBP28 W8Y data is that the decrease in splitting and intensity of the in- and out-of-phase C═O bands is due to the formation of fewer strands (e.g., a two-stranded β-sheet) compared to the number for the wild-type system. Infrared and CD measurements do not support this model. The peak at 1613 cm^{-1} is due to the turn of the first loop, indicating that the turn is formed and the strong cross-strand hydrogen bonds are in place. CD measurements of FBP28 W8Y at low temperatures show that Trp30 resides in a rigid environment, so there is also structure to the third β-sheet and the second loop. These results demonstrate that there is structure in both the first and second loop, so the decrease in splitting is not due to loss of a β-sheet. Instead, we postulate that disruption of the hydrophobic core caused by the Trp8 mutation misaligns the carbonyl oscillators in the three sheets causing the decrease in splitting and intensity.

The normalized melting curves for the WW domains derived from the temperature-dependent IR absorbance at 1634 cm^{-1} are shown in Figure 4. The data were normalized after being fit

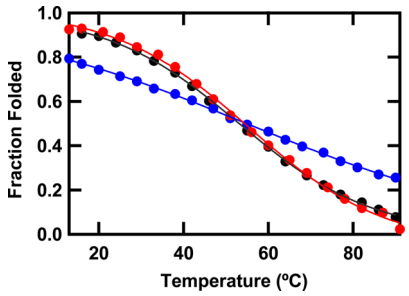

Figure 4. FTIR melt curves for FBP28 (black), FBP28 W8Y (blue), and FBP28 W30Y (red) WW domains obtained by plotting the change in IR difference spectra at 1634 cm^{-1} vs temperature. The data are fit to an apparent two-state model (eq 2) and then normalized.

to an apparent two-state equilibrium model using eq 2. The melting curve probed by infrared (Figure 4) is more broad than the melting curve probed by CD (Figure 2B) likely because infrared probes the secondary structure of the entire peptide whereas CD probes the chirality of the environment of the tryptophan residues. The melting temperatures derived from the amide I′ absorbance of FBP28 (52 ± 1 °C) and FBP28 W30Y (53 ± 1 °C) are the same within error. The melting curve derived from other wavelengths agreed with the melting temperature within the error of the fit. The fact that the melt and breadth of transitions of the FBP28 and FBP28 W30Y mutant agree supports the conclusion from the CD measurements that the Trp30 mutation does not affect the WW domain fold. The transition of FBP28 W8Y was too broad to obtain a reliable fit. This supports the observation from the FTIR and circular dichroism analysis that the W8Y mutation destabilizes the fold.

Temperature-Jump Relaxation Kinetics. The probe-dependent relaxation kinetics of the folding−unfolding transition following a laser-induced temperature jump were monitored using time-resolved infrared spectroscopy. Structure specific measurements were made using the amide I′ frequency for the amide bond vibration of the turn (1619 cm^{-1}) and residues involved in coupling between the strands of the β-sheet (1634 cm^{-1}). Jumps were performed slightly off peak center to maximize the transient absorbance signal. The complete relaxation kinetics for each peptide is reported in Tables S1 and S2 of the Supporting Information. Time-resolved measurements examined the dependence of the relaxation rates on the final temperature following a temperature jump. The magnitude of the temperature jump was kept constant while the final temperature was varied for a range of final temperatures below the melting transition. The relaxation kinetics is best fit by a triple exponential (eq 1 and Figure S2 of the Supporting Information). Figure 5 displays the relaxation

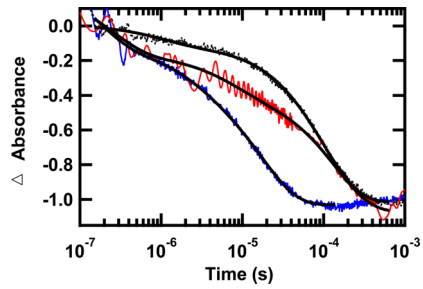

Figure 5. Representative IR T-jump relaxation kinetics of FBP28 (black), FBP28 W8Y (blue), and FBP28 W30Y (red) monitored in the amide I′ spectral region at 1634 cm^{-1} following a T-jump from 15 to 30 °C. A triple-exponential fit using eq 1 is overlaid on each kinetic trace. The data are normalized at the minimum for comparison.

kinetics of the peptides following a jump from 15 to 30 °C. The data were normalized for comparison. The fits of the data in Figure 5 are reported in Table 1. There is good agreement between the dynamics of FBP28 and the FBP28 W30Y mutant (Table S2 of the Supporting Information). Both exhibit a fast phase of hundreds of nanoseconds (τ_1), a microsecond phase (τ_2), and a slower ∼100 μs phase (τ_3). FBP28 W8Y also exhibits three phases, with the two slower phases being 1 order of magnitude faster than the other peptides. T-jump IR relaxation transients were also collected at 1661 cm^{-1} at all temperatures probed, and they exhibit three kinetic phases with the same lifetimes as those observed at 1619 and 1634 cm^{-1}. The 1661 cm^{-1} probe frequency is sensitive to disorder in the peptide, whereas the probes at 1619 and 1634 cm^{-1} report directly on specific secondary structures. Because of this, the data at 1661 cm^{-1} were useful as a control but do not provide any new information about the folding of specific secondary structures within the WW domain.

Wavelength-dependent measurements reveal differences in the dynamics of the turn of loop 1 (1619 cm^{-1}) and the β-sheet of the WW domain (1634 cm^{-1}) (Figure 6). The relaxation lifetimes observed at 1619 and 1634 cm^{-1} are similar (Tables S1 and S2 of the Supporting Information). Because there is overlap between the peaks at 1619 and 1634 cm^{-1}, probes at either location are sensitive to dynamics associated with folding at both locations, resulting in multiexponential kinetics regardless of the probe frequency. The relative amplitude of each kinetic phase depends on the probe frequency, however, which allows us to assign the structural feature that contributes most strongly to each phase. The relative amplitude of the fast phase is greatest in the transient measured at 1619 cm^{-1}, which

dx.doi.org/10.1021/bi500556h | Biochemistry 2014, 53, 5476−5484

Table 1. Relaxation Kinetics following a Temperature Jump to ~30 °C

	infrared (1634 cm^{-1})						fluorescence
	A_1 (%)	τ_1 (ns)	A_2 (%)	τ_2 (μs)	A_3 (%)	τ_3 (μs)	τ (μs)
FBP28	11 ± 4	230 ± 15	6 ± 4	9 ± 1	83 ± 1	105 ± 1	88 ± 5
FBP28 W8Y	20 ± 4	140 ± 12	15 ± 1	2.1 ± 0.2	65 ± 1	17.3 ± 0.3	22 ± 6
FBP28 W30Y	18 ± 2	320 ± 23	19 ± 2	7.4 ± 0.5	63 ± 1	143 ± 3	77 ± 4

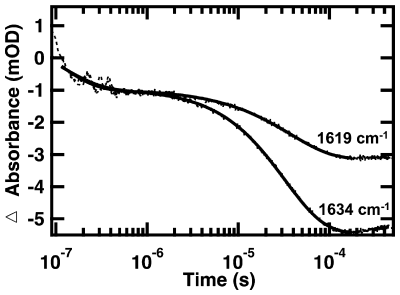

Figure 6. Representative IR *T*-jump relaxation kinetics of FBP28 monitored in the amide I′ spectral region at 1619 and 1634 cm^{-1} following a *T*-jump from 15 to 30 °C. A triple-exponential fit is overlaid on each kinetic trace (solid black lines).

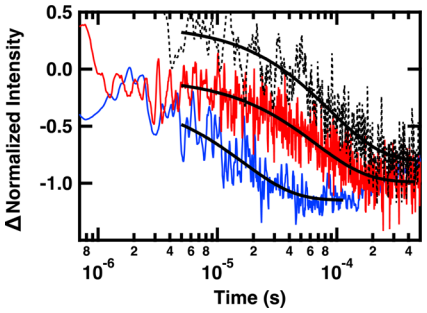

Figure 7. Representative fluorescence *T*-jump relaxation kinetics of FBP28 (black), FBP28 W30Y (red), and FBP28 W8Y (blue) excited at 285 nm and monitored at 350 nm following a *T*-jump from 20 to 28 °C. Single-exponential fits are overlaid on the kinetics traces. Data are offset for the sake of clarity.

probes the turn of loop 1. In contrast, the slower phases dominate the kinetics measured at 1634 cm^{-1}, which probes interstrand coupling across the sheet of the WW domain (Figure 6). On the basis of these observations, we assign the fast phase to turn formation in loop 1, whereas the slow phases are assigned to sheet formation. This conclusion supports the prediction from previous studies that FBP28 forms through an intermediate state in which the first hairpin is highly structured.[8,16,39]

In previous work, measurements of the FBP28 WW domain with the fast folding hairpin chignolin incorporated into the loops resulted in similar triple-exponential kinetics, where the intermediate phase is interpreted as arising from the development of the cross-strand interactions of loop 1 to form the first half of the WW domain.[18] Chignolin is a 10-residue hairpin whose sequence was optimized for stability based on the 16-residue β-hairpin G-peptide.[40] Replacing a native WW domain turn with the chignolin sequence created a difference in the stability of the two loops, which resulted in characteristic IR peaks that could be assigned to each of the loops. This made it possible to probe formation of the first and second loop separately. Because the folding of the two hairpins in the FBP28 WW domain and mutants is more cooperative, it is not possible to independently probe the dynamics of the first and second loop; however, the intermediate phase likely arises from formation of the cross-strand interactions of the first loop, because turn 1 is already formed and by analogy to the chignolin-containing system. These results support a model in which the first hairpin is formed in the intermediate state.

A second set of kinetic experiments with a series of *T*-jumps similar in magnitude was performed using time-resolved fluorescence as a probe. Figure 7 shows the relaxation kinetics for a *T*-jump from 20 to 28 °C probed by Trp fluorescence. The fits of the data in Figure 7 are listed in Table 1. The complete relaxation kinetics for each peptide and a figure demonstrating the full resolution of the fluorescence *T*-jump are reported in Figure S3 and Table S3 of the Supporting Information. In the WT and each of the mutants, we observe a single phase in the fluorescence relaxation kinetics, corresponding to the slowest IR-probed relaxation lifetime; we have already assigned the latter to folding of the second strand of the β-sheet (Figure 8). Because the fluorescence kinetics coincide

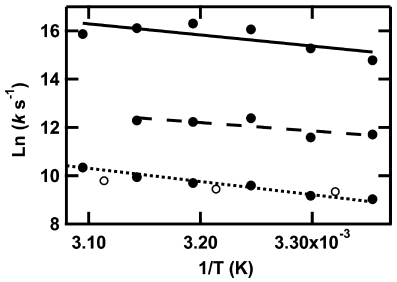

Figure 8. Arrhenius plot of the relaxation kinetics of FBP28 in the folding branch (below T_m). The values of *T* used for the 1/*T* axis are the final temperatures reached during the jump. *k* is the value obtained from a fit (see the text) of the *T*-jump transient probed by infrared at 1634 cm^{-1} (●) or fluorescence (○) spectroscopy. Lines are a results of fitting τ_1 (—), τ_2 (– – –), and τ_3 (···).

with the slowest IR phase, both report on the final step in the folding process. When the fluorescence probe is in the first loop (the W30Y mutant has a single Trp reporter, W8, in the first loop), the observed fluorescence change corresponds to the ~100 μs step. When the Trp is on the second loop (W8Y), the fluorescence transient corresponds to the ~10 μs step, but there is no slower phase in this case.

The Trp fluorescence does not report on the peptide backbone conformation (at least not directly), but rather the packing of the Trp side chains in the hydrophobic core. The Trp side chains are at least partially buried in the hydrophobic core based on the FBP28 structure (Figure 1), so the Trp fluorescence maximum reports on the formation of this core. The fluorescence spectra of FBP28 and FBP28 W30Y have similar maxima near 345 nm, typical of Trp buried in a hydrophobic environment. In contrast, the FBP28 W8Y has a decreased intensity and red-shifted maximum at 360 nm (Figure S4 of the Supporting Information), consistent with a

dx.doi.org/10.1021/bi500556h | *Biochemistry* 2014, 53, 5476−5484

more solvent-exposed Trp. The fluorescence spectrum of each of the Trp mutants is sensitive to the changes in the environment of the single remaining Trp, indicating that W8 is solvent-protected as expected from the structure (Figure 1) whereas W30 is more solvent-exposed, causing the red shift of the W8Y fluorescence spectrum. The level of solvent exposure of W30 is likely increased in the W8Y mutant because of disruption of the hydrophobic core, consistent with evidence from the IR and CD spectra. Regardless, in all cases, the fluorescence kinetics can be assigned to formation of the hydrophobic core and at least partial protection of the indole ring (or rings in the case of FBP28) from solvent. The correspondence of the fluorescence kinetics with the slowest IR phase indicates that burial of the Trp is concomitant with the folding to the native backbone topology. Therefore, the formation of the hydrophobic core depends on acquiring the native topology, meaning there is not an initial nonspecific hydrophobic collapse followed by a rearrangement to correctly align the three strands of the β-sheet structure. Importantly, this process happens faster for the W8Y mutant, which does not form a tightly packed hydrophobic core.

An intermediate dry molten globule state in which solvent has been expelled from the protein core, but having only loosely packed side chains, has been observed in several proteins.[41−46] A dry molten globule state has been observed in a protein similar to the FBP28 WW domain in size, the 35-residue villin headpiece subdomain (HP35).[47] The FBP28 W8Y mutant folds to a final state that has all of the characteristics of a dry molten globule. Its IR spectrum is consistent with a nativelike WW domain topology, having the turns and stabilizing cross-strand interactions that make up the β-sheet. Its fluorescence spectrum indicates a solvent-protected Trp30, but the critical observation is its CD spectrum, which does not have the characteristic Trp peak at 230 nm, indicating that although the Trp is buried in the core, it is disordered. We conclude that the hydrophobic core is disrupted by the Trp8 mutation and therefore does not pack tightly. The IR *T*-jump data provide further support for this model because FBP28 W8Y exhibits simplified folding kinetics, missing the slowest ~100 μs phase observed for the wild type, and the fluorescence exhibits only the ~10 μs phase. These results are consistent with a model in which the W8Y mutant folds to a dry molten globule state, but the side chains are unable to tightly pack into the final folded structure. Hydrophobic collapse to the dry molten globule state occurs on the same time scale of formation of the second loop (~10 μs). Because the FBP28 W8Y mutant does not have to search for the final closely packed side chain conformations, the folding is 1 order of magnitude faster than that of WT FBP28.

Comparison of the folding kinetics of the WT sequence with that of the W8Y mutant implies that the slow (100 μs) step in the folding of the former is tight packing of the side chains to form the native structure. Similarly, the W30Y mutant clearly folds to a nativelike structure (having the Trp 230 nm CD band and IR and fluorescence spectra nearly identical to those of the wild type) with the same kinetics as the WT sequence. Folding of the W8Y mutant occurs on the same time scale as the intermediate phase observed in the folding of the parent FBP28 and the W30Y mutant. Therefore, we assign the ~10 μs phase to formation of a dry molten globule state and the ~100 μs phase to the conversion of the dry molten globule to the tightly packed native structure as the rate-limiting step. Two different folding models involving the dry molten globule have been proposed within various systems. In the "dry molten globule hypothesis", the rate-limiting step is packing of the side chains into their native conformation from the dry molten globule.[43,44,46] In the other model, expulsion of water from the hydrophobic core to form the dry molten globule is the rate-limiting step.[41−43,45,47] Our observations support the first mechanism for FBP28, for which the tight packing of the side chains is the rate-limiting process.

Previous fluorescence *T*-jump studies of FBP28 revealed biexponential kinetics below 65 °C with relaxation lifetimes of ~30 and >900 μs.[14] In those studies, a single-point mutation, W30F, was shown to change the kinetics from biexponential to monoexponential. The interpretation of this was inconclusive, as the change could either be a reporter effect or indicate a change in the folding mechanism. We did not observe the slow >900 μs phase in our fluorescence *T*-jump measurements. A major difference in the measurements presented here is that we modified the FBP28 sequence to include point mutations designed to limit aggregation. The slow phase may have been lost because of the sensitivity of the observed kinetics to aggregation. The slow phase was also not observed in extensive studies performed by the Fersht group.[9,15,16] They concluded that the slow phase may be an early step in off-pathway aggregation, but not part of the folding mechanism. Because the FBP28 mutant that we studied was designed to eliminate aggregation, we would not expect to observe this phase.[30] The fluorescence measurements that we performed were consistent with the fast ~30 μs phase that was previously observed. Infrared measurements offer a level of detail not available from the fluorescence experiments. In particular, frequency-dependent IR measurements reveal fast nanosecond and microsecond phases not captured by fluorescence measurements. Because the infrared measurements are sensitive to changes in the peptide backbone, they are able to capture subtle changes and do not rely on a side chain reporter. This highlights the local sensitivity of infrared spectroscopy over more conventional fluorescence probes.

CONCLUSION

Using infrared spectroscopy, we are able to observe subtle differences in the time scale of formation of the turns and β-sheets of the WW domain. We propose a model to describe WW domain folding initiated in the turns, similar to that proposed for other WW domains.[8,16,18,39] Formation of the first turn initiates the formation of a two-stranded sheet from the first loop. Subsequently, the second turn and third strand fold to form the full WW domain structure. Fluorescence *T*-jump could not lead to observation of the level of detail available from infrared spectroscopy. Whereas infrared spectroscopy is sensitive to changes in the secondary structure of the protein, fluorescence spectroscopy is sensitive to the formation of the hydrophobic core, and thus, the measurements are complementary. Tryptophan mutants provide evidence of an intermediate dry molten globule state. We observe packing of the tryptophan residues on the same time scale of formation of the second loop. Thus, by utilizing multiple probes, we gain a more detailed picture of the folding landscape.

ASSOCIATED CONTENT

Supporting Information

Temperature-dependent FTIR spectra of FBP28 W8Y and FBP28 W30Y, equilibrium fluorescence, residuals from transient fits, and a complete table of relaxation kinetics for

FBP28, FBP28 W8Y, and FBP28 W30Y probed by infrared and fluorescence spectroscopy. This material is available free of charge via the Internet at http://pubs.acs.org.

AUTHOR INFORMATION

Corresponding Author

*E-mail: briandyer@emory.edu.

Funding

This work was supported by National Institutes of Health Grant R01 GM53640 to R.B.D.

Notes

The authors declare no competing financial interest.

REFERENCES

(1) Culik, R. M., Serrano, A. L., Bunagan, M. R., and Gai, F. (2011) Achieving Secondary Structural Resolution in Kinetic Measurements of Protein Folding: A Case Study of the Folding Mechanism of Trp-cage. *Angew. Chem., Int. Ed. 50*, 10884−10887.

(2) Vu, D. M., Brewer, S. H., and Dyer, R. B. (2012) Early turn formation and chain collapse drive fast folding of the major cold shock protein CspA of *Escherichia coli*. *Biochemistry 51*, 9104−9111.

(3) Macias, M. J., Hyvonen, M., Baraldi, E., Schultz, J., Sudol, M., Saraste, M., and Oschkinat, H. (1996) Structure of the WW domain of a kinase-associated protein complexed with a proline-rich peptide. *Nature 382*, 646−649.

(4) Macias, M. J., Gervais, V., Civera, C., and Oschkinat, H. (2000) Structural analysis of WW domains and design of a WW prototype. *Nat. Struct. Biol. 7*, 375−379.

(5) Verdecia, M. A., Bowman, M. E., Lu, K. P., Hunter, T., and Noel, J. P. (2000) Structural basis for phosphoserine-proline recognition by group IVWW domains. *Nat. Struct. Biol. 7*, 639−643.

(6) Wiesner, S., Stier, G., Sattler, M., and Macias, M. J. (2002) Solution structure and ligand recognition of the WW domain pair of the yeast splicing factor Prp40. *J. Mol. Biol. 324*, 807−822.

(7) Piana, S., Sarkar, K., Lindorff-Larsen, K., Guo, M. H., Gruebele, M., and Shaw, D. E. (2011) Computational Design and Experimental Testing of the Fastest-Folding β-Sheet Protein. *J. Mol. Biol. 405*, 43−48.

(8) Jager, M., Nguyen, H., Crane, J. C., Kelly, J. W., and Gruebele, M. (2001) The folding mechanism of a β-sheet: The WW domain. *J. Mol. Biol. 311*, 373−393.

(9) Ferguson, N., Johnson, C. M., Macias, M., Oschkinat, H., and Fersht, A. (2001) Ultrafast folding of WW domains without structured aromatic clusters in the denatured state. *Proc. Natl. Acad. Sci. U.S.A. 98*, 13002−13007.

(10) Karanicolas, J., and Brooks, C. L., III (2003) The structural basis for biphasic kinetics in the folding of the WW domain from a formin-binding protein: Lessons for protein design? *Proc. Natl. Acad. Sci. U.S.A. 100*, 3954−3959.

(11) Karanicolas, J., and Brooks, C. L. (2004) Integrating folding kinetics and protein function: Biphasic kinetics and dual binding specificity in a WW domain. *Proc. Natl. Acad. Sci. U.S.A. 101*, 3432−3437.

(12) Mu, Y. G., Nordenskiold, L., and Tam, J. P. (2006) Folding, misfolding, and amyloid protofibril formation of WW domain FBP28. *Biophys. J. 90*, 3983−3992.

(13) Noe, F., Schutte, C., Vanden-Eijnden, E., Reich, L., and Weikl, T. R. (2009) Constructing the equilibrium ensemble of folding pathways from short off-equilibrium simulations. *Proc. Natl. Acad. Sci. U.S.A. 106*, 19011−19016.

(14) Nguyen, H., Jager, M., Moretto, A., Gruebele, M., and Kelly, J. W. (2003) Tuning the free-energy landscape of a WW domain by temperature, mutation, and truncation. *Proc. Natl. Acad. Sci. U.S.A. 100*, 3948−3953.

(15) Ferguson, N., Berriman, J., Petrovich, M., Sharpe, T. D., Finch, J. T., and Fersht, A. R. (2003) Rapid amyloid fiber formation from the fast-folding WW domain FBP28. *Proc. Natl. Acad. Sci. U.S.A. 100*, 9814−9819.

(16) Petrovich, M., Jonsson, A. L., Ferguson, N., Daggett, V., and Fersht, A. R. (2006) φ-Analysis at the experimental limits: Mechanism of β-hairpin formation. *J. Mol. Biol. 360*, 865−881.

(17) Liu, F., Du, D. G., Fuller, A. A., Davoren, J. E., Wipf, P., Kelly, J. W., and Gruebele, M. (2008) An experimental survey of the transition between two-state and downhill protein folding scenarios. *Proc. Natl. Acad. Sci. U.S.A. 105*, 2369−2374.

(18) Davis, C. M., and Dyer, R. B. (2013) Dynamics of an ultrafast folding subdomain in the context of a larger protein fold. *J. Am. Chem. Soc. 135*, 19260−19267.

(19) Chung, H. S., McHale, K., Louis, J. M., and Eaton, W. A. (2012) Single-Molecule Fluorescence Experiments Determine Protein Folding Transition Path Times. *Science 335*, 981−984.

(20) Andrushchenko, V. V., Vogel, H. J., and Prenner, E. J. (2007) Optimization of the hydrochloric acid concentration used for trifluoroacetate removal from synthetic peptides. *J. Pept. Sci. 13*, 37−43.

(21) Williams, S., Causgrove, T. P., Gilmanshin, R., Fang, K. S., Callender, R. H., Woodruff, W. H., and Dyer, R. B. (1996) Fast events in protein folding: Helix melting and formation in a small peptide. *Biochemistry 35*, 691−697.

(22) Manning, M. C., and Woody, R. W. (1987) Theoretical Determination of the CD of Proteins Containing Closely Packed Antiparallel β-Sheets. *Biopolymers 26*, 1731−1752.

(23) Koepf, E. K., Petrassi, H. M., Sudol, M., and Kelly, J. W. (1999) WW: An isolated three-stranded antiparallel β-sheet domain that unfolds and refolds reversibly; evidence for a structured hydrophobic cluster in urea and GdnHCl and a disordered thermal unfolded state. *Protein Sci. 8*, 841−853.

(24) Koepf, E. K., Petrassi, H. M., Ratnaswamy, G., Huff, M. E., Sudol, M., and Kelly, J. W. (1999) Characterization of the structure and function of W → FWW domain variants: Identification of a natively unfolded protein that folds upon ligand binding. *Biochemistry 38*, 14338−14351.

(25) Viguera, A. R., Arrondo, J. L., Musacchio, A., Saraste, M., and Serrano, L. (1994) Characterization of the interaction of natural proline-rich peptides with five different SH3 domains. *Biochemistry 33*, 10925−10933.

(26) Knapp, S., Mattson, P. T., Christova, P., Berndt, K. D., Karshikoff, A., Vihinen, M., Smith, C. I., and Ladenstein, R. (1998) Thermal unfolding of small proteins with SH3 domain folding pattern. *Proteins 31*, 309−319.

(27) Reid, K. L., Rodriguez, H. M., Hillier, B. J., and Gregoret, L. M. (1998) Stability and folding properties of a model β-sheet protein, *Escherichia coli* CspA. *Protein Sci. 7*, 470−479.

(28) Kraemer-Pecore, C. M., Lecomte, J. T. J., and Desjarlais, J. R. (2003) A de novo redesign of the WW domain. *Protein Sci. 12*, 2194−2205.

(29) Nicholson, E. M., and Scholtz, J. M. (1996) Conformational stability of the *Escherichia coli* HPr protein: Test of the linear extrapolation method and a thermodynamic characterization of cold denaturation. *Biochemistry 35*, 11369−11378.

(30) Tremmel, S., Beyermann, M., Oschkinat, H., Bienert, M., Naumann, D., and Fabian, H. (2005) C-13-labeled tyrosine residues as local IR probes for monitoring conformational changes in peptides and proteins. *Angew. Chem., Int. Ed. 44*, 4631−4635.

(31) Yang, W. J., Griffiths, P. R., Byler, D. M., and Susi, H. (1985) Protein Conformation by Infrared-Spectroscopy: Resolution Enhancement by Fourier Self-Deconvolution. *Appl. Spectrosc. 39*, 282−287.

(32) Arrondo, J. L. R., Blanco, F. J., Serrano, L., and Goni, F. M. (1996) Infrared evidence of a β-hairpin peptide structure in solution. *FEBS Lett. 384*, 35−37.

(33) Susi, H., and Byler, D. M. (1986) Resolution-Enhanced Fourier-Transform Infrared-Spectroscopy of Enzymes. *Methods Enzymol. 130*, 290−311.

(34) Wang, T., Xu, Y., Du, D. G., and Gai, F. (2004) Determining β-sheet stability by Fourier transform infrared difference spectra. *Biopolymers 75*, 163−172.
(35) Hilario, J., Kubelka, J., and Keiderling, T. A. (2003) Optical spectroscopic investigations of model β-sheet hairpins in aqueous solution. *J. Am. Chem. Soc. 125*, 7562−7574.
(36) Maness, S. J., Franzen, S., Gibbs, A. C., Causgrove, T. P., and Dyer, R. B. (2003) Nanosecond temperature jump relaxation dynamics of cyclic β-hairpin peptides. *Biophys. J. 84*, 3874−3882.
(37) Chan, D. C., Bedford, M. T., and Leder, P. (1996) Formin binding proteins bear WWP/WW domains that bind proline-rich peptides and functionally resemble SH3 domains. *EMBO J. 15*, 1045−1054.
(38) Kubelka, J., and Keiderling, T. A. (2001) Differentiation of β-sheet-forming structures: Ab initio-based simulations of IR absorption and vibrational CD for model peptide and protein β-sheets. *J. Am. Chem. Soc. 123*, 12048−12058.
(39) Deechongkit, S., Nguyen, H., Powers, E. T., Dawson, P. E., Gruebele, M., and Kelly, J. W. (2004) Context-dependent contributions of backbone hydrogen bonding to β-sheet folding energetics. *Nature 430*, 101−105.
(40) Honda, S., Kobayashi, N., and Munekata, E. (2000) Thermodynamics of a β-hairpin structure: Evidence for cooperative formation of folding nucleus. *J. Mol. Biol. 295*, 269−278.
(41) Baldwin, R. L., Frieden, C., and Rose, G. D. (2010) Dry molten globule intermediates and the mechanism of protein unfolding. *Proteins 78*, 2725−2737.
(42) Jha, S. K., and Udgaonkar, J. B. (2009) Direct evidence for a dry molten globule intermediate during the unfolding of a small protein. *Proc. Natl. Acad. Sci. U.S.A. 106*, 12289−12294.
(43) Levitt, M., Gerstein, M., Huang, E., Subbiah, S., and Tsai, J. (1997) Protein folding: The endgame. *Annu. Rev. Biochem. 66*, 549−579.
(44) Shakhnovich, E. I., and Finkelstein, A. V. (1989) Theory of Cooperative Transitions in Protein Molecules. 1. Why Denaturation of Globular Protein Is a 1st-Order Phase-Transition. *Biopolymers 28*, 1667−1680.
(45) Kiefhaber, T., Labhardt, A. M., and Baldwin, R. L. (1995) Direct NMR Evidence for an Intermediate Preceding the Rate-Limiting Step in the Unfolding of Ribonuclease-A. *Nature 375*, 513−515.
(46) Hoeltzli, S. D., and Frieden, C. (1995) Stopped-Flow NMR-Spectroscopy: Real-Time Unfolding Studies of 6-F-19-Tryptophan-Labeled *Escherichia coli* Dihydrofolate-Reductase. *Proc. Natl. Acad. Sci. U.S.A. 92*, 9318−9322.
(47) Reiner, A., Henklein, P., and Kiefhaber, T. (2010) An unlocking/relocking barrier in conformational fluctuations of villin headpiece subdomain. *Proc. Natl. Acad. Sci. U.S.A. 107*, 4955−4960.